A&A 617, A87 (2018)
https://doi.org/10.1051/0004-6361/201833439

Astronomy & Astrophysics

H_2 chemistry in interstellar ices: the case of CO ice hydrogenation in UV irradiated CO:H_2 ice mixtures

K.-J. Chuang[1,2], G. Fedoseev[3], D. Qasim[1], S. Ioppolo[4,5], E. F. van Dishoeck[2], and H. Linnartz[1]

[1] Sackler Laboratory for Astrophysics, Leiden Observatory, Leiden University, PO Box 9513, 2300 RA Leiden, The Netherlands
e-mail: chuang@strw.leidenuniv.nl
[2] Leiden Observatory, Leiden University, PO Box 9513, 2300 RA Leiden, The Netherlands
[3] INAF – Osservatorio Astrofisico di Catania, via Santa Sofia 78, 95123 Catania, Italy
[4] School of Electronic Engineering and Computer Science, Queen Mary University of London, Mile End Road, London E1 4NS, UK
[5] School of Physical Sciences, The Open University, Walton Hall, Milton Keynes MK7 6AA, UK

Received 16 May 2018 / Accepted 11 July 2018

ABSTRACT

Context. In dense clouds, hydrogenation reactions on icy dust grains are key in the formation of molecules, like formaldehyde, methanol, and complex organic molecules (COMs). These species form through the sequential hydrogenation of CO ice. Although molecular hydrogen (H_2) abundances can be four orders of magnitude higher than those of free H-atoms in dense clouds, H_2 surface chemistry has been largely ignored; several laboratory studies show that H_2 does not actively participate in "non-energetic" ice chemistry because of the high activation energies required.

Aims. For the example of CO ice hydrogenation, we experimentally investigated the potential role of H_2 molecules on the surface chemistry when "energetic" processing (i.e., UV photolysis) is involved. We test whether additional hydrogenation pathways become available upon UV irradiation of a CO:H_2 ice mixture and whether this reaction mechanism also applies to other chemical systems.

Methods. Ultra-high vacuum (UHV) experiments were performed at 8–20 K. A pre-deposited solid mixture of CO:H_2 was irradiated with UV-photons. Reflection absorption infrared spectroscopy (RAIRS) was used as an in situ diagnostic tool. Single reaction steps and possible isotopic effects were studied by comparing results from CO:H_2 and CO:D_2 ice mixtures.

Results. After UV-irradiation of a CO:H_2 ice mixture, two photon-induced products, HCO and H_2CO, are unambiguously detected. The proposed reaction mechanism involves electronically excited CO in the following reaction steps: $CO + h\nu \longrightarrow CO^*$, $CO^* + H_2 \longrightarrow HCO + H$ where newly formed H-atoms are then available for further hydrogenation reactions. The HCO formation yields have a strong temperature dependence for the investigated regime, which is most likely linked to the H_2 sticking coefficient. Moreover, the derived formation cross section reflects a cumulative reaction rate that mainly determined by both the H-atom diffusion rate and initial concentration of H_2 at 8–20 K and that is largely determined by the H_2 sticking coefficient. Finally, the astronomical relevance of this photo-induced reaction channel is discussed.

Key words. astrochemistry – methods: laboratory: solid state – infrared: ISM – ultraviolet: ISM – ISM: molecules – molecular processes

1. Introduction

In dense molecular clouds, carbon monoxide starts heavily accreting on H_2O-rich ice mantles when densities (i.e., n_H=$2n(H_2)+n(H)$) increase to $\sim 10^{4-5}$ cm^{-3}, and temperatures drop to ∼10 K. This results in a CO-rich ice coating with a thickness of ∼0.01 μm (Pontoppidan 2006; Boogert et al. 2015) and is known as the "CO catastrophic freeze-out stage". During this stage, the simultaneous accretion of H-atoms and CO leads primarily to the formation of H_2CO and CH_3OH through successive H-atom addition reactions $CO \xrightarrow{H} HCO \xrightarrow{H} H_2CO \xrightarrow{H} CH_3O \xrightarrow{H} CH_3OH$ as introduced in gas-grain models by Tielens & Hagen (1982). These hydrogenation reactions have been investigated in a number of systematic laboratory experiments (Watanabe & Kouchi 2002; Fuchs et al. 2009, see reviews by Watanabe & Kouchi 2008; Hama & Watanabe 2013; Linnartz et al. 2015) as well as astrochemical simulations and theoretical studies (Charnley 1997; Cuppen et al. 2009; Chang & Herbst 2012). The CO + H channel is also regarded as a starting point in the formation of various complex organic molecules (COMs) in dense clouds; recombination of reactive intermediates –HCO, CH_2OH, and CH_3O, formed in H-atom addition and abstraction reactions with each other or with other reaction products results in the low temperature solid-state formation of larger COMs, like glycolaldehyde, ethylene glycol, glycerol, and likely glyceraldehyde (Garrod et al. 2006; Woods et al. 2012; Butscher et al. 2015, 2016; Fedoseev et al. 2015, 2017; Chuang et al. 2016, 2017). The astronomical gas-phase detection of a number of COMs in cold dark regions, that is, environments in which (UV) photo-processing is not dominant, has been explained in this way (Öberg et al. 2010; Bacmann et al. 2012; Cernicharo et al. 2012; Jiménez-Serra et al. 2016), even though the mechanism transferring the solid COMs into the gas phase is still not fully understood (Balucani et al. 2015; Bertin et al. 2016; Chuang et al. 2018; Ligterink et al. 2018). Key in all this work is the important role of accreting H-atoms.

Molecular hydrogen, H_2, is the most abundant molecule in the Universe (Wooden et al. 2004). Particularly in molecular clouds, the gaseous abundance of H_2 is about four orders of magnitude higher than that of CO and H-atoms. Molecular hydrogen

may freeze out and the direct observation of H_2 ice was claimed by Sandford et al. (1993) in the infrared spectrum of WL5 in the ρ Oph molecular cloud, thanks to a small induced dipole as a result of H_2 interacting with surrounding ice species (Warren et al. 1980). Later on this observation was questioned (Kristensen et al. 2011). It is, however, widely accepted that H_2 is abundantly formed in the solid state through H–H recombination on silicate or carbonaceous dust grains or amorphous water ice, through photolysis of hydrogenated amorphous carbon or water, or H_2 abstraction from polycyclic aromatic hydrocarbons (see reviews by Vidali 2013; Wakelam et al. 2017, and references therein). Which of these formation mechanisms dominates, depends on the environmental conditions (Wakelam et al. 2017).

H_2 is extremely volatile, and its sticking coefficient, which is defined as the ratio of "adsorbed-species" to "total incident-species" for a given period of time, is a function of several properties, for example, binding energy of adsorbed species on a surface, species coverage, and substrate temperature (Hama & Watanabe 2013). This coefficient also depends on the incident energy and angle of impacting species (Matar et al. 2010). Given the very small binding energy ($E_b \sim 100$ K) of H_2 accreting on a preformed H_2 ice layer, multilayer "pure" H_2 ice is not expected under dense cloud conditions (Lee 1972). However, in space, ice mantles formed by condensation on grain surfaces are typically amorphous, resulting in a distribution of binding energies. In a three-dimensional off-lattice Monte Carlo simulation, Garrod (2013) found that the water ice formation on grain surfaces exhibits a highly porous (creviced) structure. Sites with relatively high binding energies in these pores can be a place where H_2 sticks (Buch & Devlin 1994). Laboratory results by Dissly et al. (1994) showed that H_2 can accrete together with other interstellar species, such as H_2O, under dense cloud conditions with an ice ratio (H_2:H_2O) of ~0.3. However, a gas phase co-deposition of H_2O and H_2 in the interstellar medium (ISM) is unlikely due to the low density of gaseous H_2O for the temperatures at which H_2 starts freezing-out. Moreover, it is well established that H_2O is mainly produced in situ on grain surfaces through the hydrogenation of oxygen allotropes accreting from the gas phase prior to gaseous CO condensation (Hiraoka et al. 1998; Ioppolo et al. 2008; Miyauchi et al. 2008; Oba et al. 2009; Cuppen et al. 2010; Dulieu et al. 2010; Ioppolo et al. 2010; Oba et al. 2012; Lamberts et al. 2013). In recent laboratory studies, the reported H_2 sticking coefficients in a sub-monolayer regime on an olivine sample (i.e., a magnesium iron silicate) showed an unexpectedly high value of ~0.7 at 10 K (Acharyya 2014). This hints for the possibility that gaseous H_2 could co-deposit with other species on dust grains at low temperature and in particular with CO, forming CO:H_2 ice mantles, during its catastrophic freeze-out stage. In principle, this could facilitate reactions between CO and H_2, however, as ground-state molecule–molecule reactions typically have a very high activation energy and are often endothermic, even the four orders of magnitude higher H_2 abundance compared to atomic hydrogen is not expected to compensate for the high reaction barriers.

At high visual extinctions (A_V), dark clouds are shielded from external UV radiation by the dust. Only cosmic rays are expected to penetrate the cloud and react with the abundant gaseous H_2, resulting in the emission of UV photons. The internal cloud UV-photon flux is $(1-10)\times10^3$ photons cm^{-2} s^{-1}, which is a few times lower than the typical H-atom flux in the same regions (Prasad & Tarafdar 1983; Mennella et al. 2003; Shen et al. 2004). However, UV-photons have a larger penetration depth in interstellar ice analogues, for instance, 830 ML in H_2O and 640 ML in CO, with 95% absorption for 120–160 nm (Cruz-Diaz et al. 2014). The energy of these UV-photons (mainly located around 160 and at 121.6 nm, i.e., Lyα) is not high enough to directly dissociate H_2 or CO, but is sufficient to radiatively pump CO (i.e., $A^1\Pi \longleftarrow X^1\Sigma^+$) into a vibronically excited state, CO* (Tobias et al. 1960). This energy can be transferred from subsurface layers to eject CO molecules located in the first few top-layers resulting in a CO photo-desorption event, following a so called DIET (Desorption Induced by Electronic Transition) mechanism (Fayolle et al. 2011; Bertin et al. 2013; van Hemert et al. 2015). Alternatively, this energy can be used to overcome the activation energy of the involved barriers resulting in the formation of photo-products, such as CO_2 (Gerakines et al. 1996; Gerakines & Moore 2001; Loeffler et al. 2005).

The present work is motivated by our limited understanding of the impact of UV-photons interacting with H_2-containing ices under dense cloud conditions. The idea of studying the role of molecular hydrogen in grain surface chemistry is not new. Previous work, like Fuchs et al. (2009) excluded the direct role of H_2 in the formation of H_2CO and CH_3OH. Oba et al. (2012) proposed a H_2O formation mechanism through the reactions between H_2 and OH radical, and found isotope effects when using D_2 instead of H_2 (see also Meisner et al. 2017). Recently, Lamberts et al. (2014) experimentally studied the reaction between H_2 and O in the ground state to form H_2O on grain surfaces, and this only resulted in a rather low upper limit for H_2O formation for this channel in dense clouds. A similar mechanism was also studied to explain the HCN formation through the reaction $H_2 + CN$ in an H_2 matrix experiment (Borget et al. 2017). Here, we focus on the UV irradiation of a CO:H_2 ice mixture studied for temperatures ranging from 8 to 20 K. The aim is to investigate whether cosmic ray-induced UV-photons can trigger surface reactions between an electronically excited species, for example, CO in this work, and H_2, the two most abundant molecules in prestellar cores, and how this compares to the regular CO ice H-atom addition reaction scheme.

2. Experimental

All experiments were performed by using SURFRESIDE[2], an ultra-high vacuum (UHV) setup, which has been described in detail in Ioppolo et al. (2013). The base pressure of the main chamber is $\sim10^{-10}$ mbar, and the H_2O contamination from the residual gas accretion, which is observed by its monomer IR feature at 1600 cm^{-1}, is estimated to be $<3\times10^{10}$ molecules cm^{-2} s^{-1}. A gold-plated copper substrate is centered in the chamber and cooled by a closed-cycle helium cryostat that allows for variation of the substrate temperature between 8 and 450 K, which is monitored by two silicon diode thermal sensors with 0.5 K absolute accuracy. Gaseous species, that are H_2 (D_2; Linde 5.0) and CO (Linde 2.0), are separately introduced into the UHV chamber through the Hydrogen Atom-Beam Source line (filament is off and at room temperature) and a molecule dosing line, respectively. The ice sample is monitored in situ, before and during UV-photon irradiation by Fourier Transform Reflection-Absorption InfraRed Spectroscopy (FT-RAIRS) in the range from 700 to 4000 cm^{-1}, with 1 cm^{-1} resolution. The RAIR band strength value of CO and possible formation products, like H_2CO is obtained from the laser interference experiments described by Chuang et al. (2018). The HCO radical band strength value for RAIRS is calibrated from the averaged transmission value estimated by Bennett et al. (2007) and Gerakines et al. (1996) multiplying a conversion factor (i.e., the ratio of "reflection mode" to "transmission mode" is 4.7 for present IR setting). The conversion factor is based on the assumption that the band strength ratio

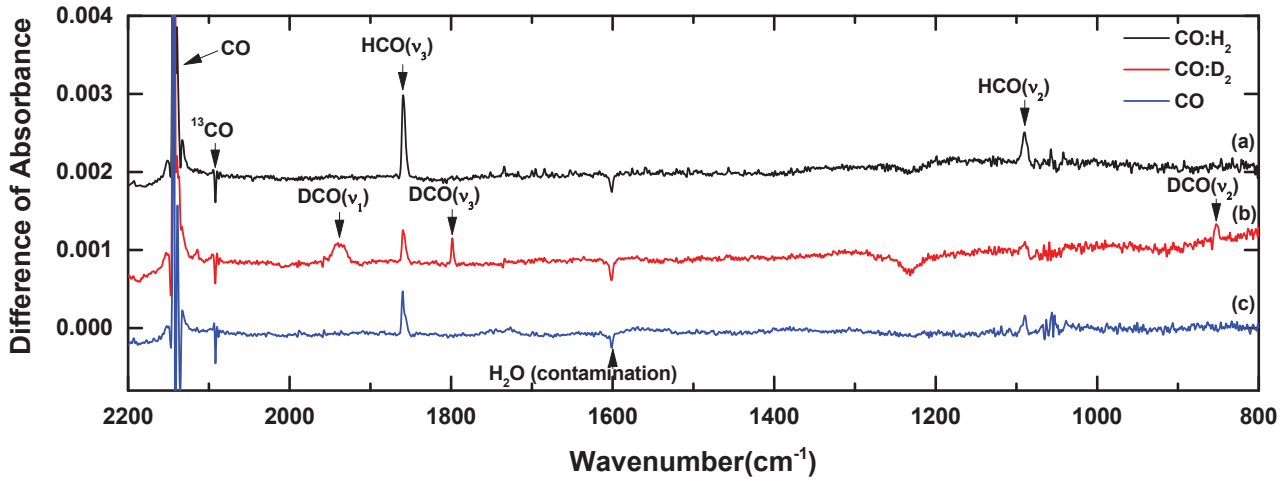

Fig. 1. IR difference spectra obtained after UV irradiation of pre-deposited (*a*) CO:H_2, (*b*) CO:D_2, and (*c*) CO ice with a photon-flux of 6×10^{12} photons cm^{-2} s^{-1} over 60 min at 8 K.

of HCO to CO is constant in both transmission and reflection IR spectroscopy (Öberg et al. 2009). Since the DCO band strength has not been reported in the literature, it is estimated by multiplying the HCO band strength value with a factor of 1.35. This conversion factor is obtained under the assumption that the band strength ratio in C=O stretching mode of DCO to HCO is similar to the ratio of D_2CO to H_2CO (i.e., 1.35) reported in Hidaka et al. (2009) . The used IR band strengths in this work are 5.2×10^{-17}, 5.7×10^{-17}, 7.7×10^{-17}, and 8.3×10^{-17} cm molecule^{-1} for CO (2142 cm^{-1}), HCO (1859 cm^{-1}), DCO (1798 cm^{-1}), and H_2CO (1737 cm^{-1}), respectively. The deposition rate of CO ice is 1.7×10^{13} molecules cm^{-2} s^{-1} determined by using a modified Beer–Lambert law for the IR absorbance at 2142 cm^{-1}. As H_2 (D_2) is an IR inactive molecule, the H_2 (D_2) exposure rate is obtained by the Langmuir estimation (i.e., 1×10^6 torr·s = 1 L) resulting in a flux through the substrate plane of 7.3×10^{14} molecules cm^{-2} s^{-1}. The H_2 sticking coefficient (f) on pure CO ice is not available from the literature, and is expected to depend strongly on temperatures in the range of 8–20 K. Moreover, not all the H_2 that gets temporarily stuck will stay on the surface long enough to also get trapped in the bulk of the ice; the residence time of H_2 on the surface is limited which causes a fraction to return into the gas phase. Therefore, the estimated concentration of H_2 ice is an upper limit and expected to be less than CO due to the very small binding energy for multilayer H_2 ice. The ice deposition time is 60 min resulting in a very similar column density of CO in all experiments.

After the simultaneous deposition of a CO:H_2 ice mixture, UV photons generated by a Microwave Discharge Hydrogen flowing Lamp (MDHL) are guided through a MgF_2 window onto the ice sample at a 90 degrees angle with respect to the ice layer covering the entire substrate area (2.5×2.5 cm^2). The spectral emission pattern and fluxes have been characterized in detail in previous work (Ligterink et al. 2015; Fedoseev et al. 2016; Chuang et al. 2017). The used H_2 pressure amounts to ~1 mbar which corresponds to a ratio of "Lyα" to "H_2-emission (~160 nm)"≅ 1.7 and UV-photon flux of $\sim 6 \times 10^{12}$ photons cm^{-2} s^{-1} (Ligterink et al. 2015).

3. Results

3.1. HCO formation

Figure 1 presents the IR difference spectra obtained after UV-photon irradiation of pre-deposited (a) CO:H_2, (b) CO:D_2, and (c) pure CO ice at 8 K with a photon-flux of 6×10^{12} photons cm^{-2} s^{-1} for 60 min. The negative peaks visible at 2142 and 2091 cm^{-1} are due to CO and its natural isotope ^{13}CO, respectively, and reflect that their initial ice abundances decrease through photo-desorption and photo-chemistry. H_2 consumption cannot be monitored by using RAIRS; in the infrared, frozen H_2 can only be made visible through transitions at 4137 and 4144 cm^{-1} that are the result of a small dipole moment induced through interactions with CO ice (Warren et al. 1980). The estimated band strength, however, is extremely small, that is $\sim 10^{-19}$ cm molecule^{-1} and about two orders of magnitude smaller than for CO ice (Sandford & Allamandola 1993). For the relatively thin ices studied in our experiments, therefore, it is not possible to monitor H_2 directly.

The positive peaks at 1859, 1090, and 2488 cm^{-1} (the latter is not shown in Fig. 1) in the CO:H_2 experiment indicate the formation of HCO, and originate from its C–O stretching (ν_3), bending (ν_2), and C–H stretching (ν_1) vibration mode, respectively (Ewing et al. 1960; Milligan & Jacox 1964). The corresponding isotopic product of the formyl radical (DCO) in the CO:D_2 experiment is identified by absorption signals at 1798, 852, and 1938 cm^{-1} due to its C–O stretching (ν_3), bending (ν_2), and C–D stretching (ν_1) vibrational modes, respectively (Ewing et al. 1960; Milligan & Jacox 1964). In experiments (b) and (c), HCO peaks can also be observed. The HCO features in (b) and (c) are weaker than in (a) and can be explained by the presence of H_2 or H_2O as background residual gases in the UHV chamber. This is confirmed by the fact that the HCO feature strengths are identical in experiments (b) and (c). Since no DCO signal is found in experiment (a) we confirm the formation of HCO(DCO) upon UV irradiation of a CO:H_2(CO:D_2) ices. The estimated H_2O column density, that is $N(H_2O)$, is below $\sim 0.1 \times 10^{15}$ molecules cm^{-2} in all three experiments and the ratio of $N(H_2O)/N_{\rm deposited}(CO) < 0.002$ after CO:H_2 ice mixture preparation. Other photolysis products, like CO_2 (2346 cm^{-1}) and its isotope $^{13}CO_2$ (2280 cm^{-1}) are also detected in all three experiments (not shown in Fig. 1). Their formation has been reported in previous UV-photon irradiation studies of pure CO ice (Gerakines et al. 1995; Gerakines & Moore 2001; Muñoz Caro et al. 2010; Chen et al. 2014; Paardekooper et al. 2016). The initial ice thickness of CO is beyond the RAIRS saturation limit for our experimental conditions, making it difficult to quantify the CO column density directly from its IR absorbance signal at 2142 cm^{-1}. Given the constant CO:^{13}CO ratio (i.e., the natural

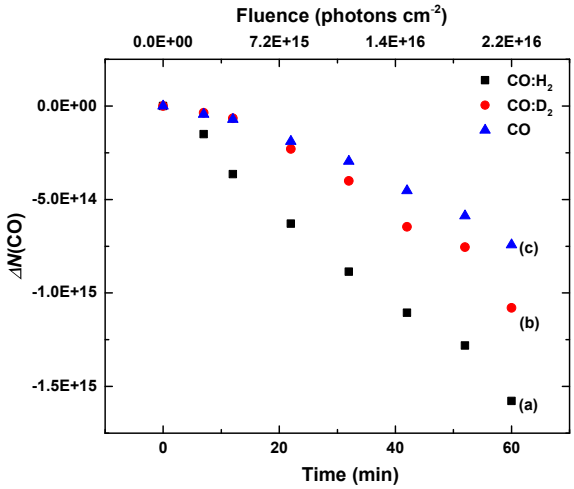

Fig. 2. Evolution of the ΔN(CO) depletion over 60 min of UV-photon irradiation with a photon-flux of 6×10^{12} photons cm^{-2} s^{-1} at 8 K for (a) CO:H_2, (b) CO:D_2, and (c) CO ice. The ΔN(CO) has been calibrated by the initial ^{13}CO ice thickness.

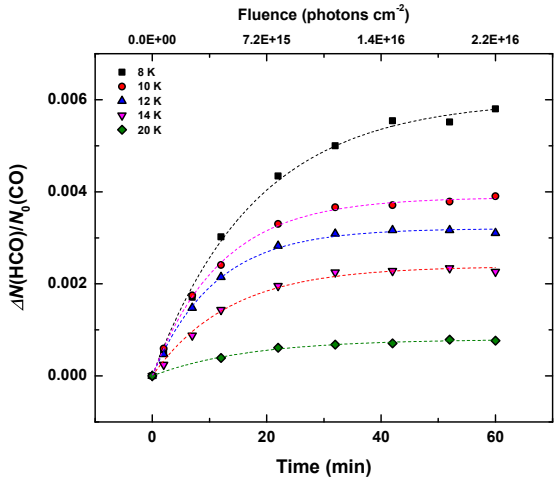

Fig. 3. Evolution of the newly formed N(HCO) w.r.t. initially predeposited N_0(CO) over 60 min of UV-photon irradiation of CO + H_2 ice mixture with a photon-flux of 6×10^{12} photons cm^{-2} s^{-1} at 8, 10, 12, 14, and 20 K, respectively. The dashed lines are the exponentially fitted results by using Eq. (1).

abundance of CO:^{13}CO = 98.9:1.1), the unsaturated ^{13}CO feature can also be used to derive the CO abundance. Figure 2 shows the relative intensity changes of the CO abundance during 60 min of UV-photon irradiation at 8 K for the three experiments shown in Fig. 1, that is ΔN(CO), determined from the integrated IR absorbance area of ^{13}CO (2091 cm^{-1}). In all three experiments, the CO abundance is clearly decreasing; after 60 min of UV photolysis which corresponds to a UV fluence of 2.2×10^{16} photons cm^{-2}, the depletion ΔN(CO) is 1.6×10^{15}, 1.1×10^{15}, and 0.7×10^{15} molecules cm^{-2} for (a) CO:H_2, (b) CO:D_2, and (c) CO ice, respectively.

The UV-photon irradiation of pure CO ice has been extensively studied; CO ice is mainly found to photo-desorb following a DIET mechanism and small amounts of CO_2 at the level of a few percent are formed in the ice (see for an overview Paardekooper et al. 2016). After calibrating the distance between the ice sample and MDHL, and assuming that the light acts as a point source, the absolute depletion rate per second of pure CO ice is derived as 4.9×10^{11} molecules cm^{-2} s^{-1}, comparable to the rate of $(3.2 \pm 1.7) \times 10^{11}$ molecules cm^{-2} s^{-1} reported in Paardekooper et al. (2016) for very similar MDHL settings. The derived absolute CO photo-desorption rate is 3.2×10^{-2} molecules photon^{-1} by employing the photon flux used in this work. The experimental CO absolute depletion rates for CO:H_2 and CO:D_2 ices are ~2 and ~1.5 times higher, respectively, indicating that more CO has been consumed than can be explained by photo-desorption only, namely, this observation is fully consistent with additional CO losses because of involvement in photo-chemical reactions with H_2 (D_2) forming HCO (DCO), as shown in Fig. 1.

3.2. Temperature dependence

Figure 3 presents the column density of N(HCO) obtained from the integration of the IR feature at 1859 cm^{-1} and normalized to the initial CO abundance, that is N_0(CO), for experiments of CO:H_2 ice over 60 min UV-photon irradiation at 8, 10, 12, 14, and 20 K. The HCO production grows with increasing UV-photon fluence impinging on the ice mixture, and reaches saturation around 30–60 min (except at 8 K), which implies that a balance between HCO formation and destruction processes is eventually reached. The final HCO abundances after 60 min of UV-photon irradiation show a strong temperature dependence in the range of 8–20 K; at 20 K, the yield of HCO is only ~10% of the production at 8 K. Because of the small absorption cross section reported for CO, that is 4.7×10^{-18} cm^2 (Cruz-Diaz et al. 2014), and as the energy dissipation lifetime is relatively short (~15 ns; Chervenak & Anderson 1971), here, we assume that the electronically excited CO triggered by impinging UV-photons is the limited reactant. Under the steady-state approximation the ΔN(HCO)/N_0(CO) formation yield can be described by the following pseudo-first order kinetic equation (Watanabe et al. 2006; Hidaka et al. 2007):

$$\frac{\Delta N(\mathrm{HCO})}{N_0(\mathrm{CO})} = \alpha(1 - \exp(-N(\mathrm{H_2}) \cdot k \cdot t)) = \alpha(1 - \exp(-\phi \cdot \sigma \cdot t)), \quad (1)$$

where $N(H_2)$ is the column density of hydrogen molecules in molecules cm^{-2}, k is the rate constant in cm^2 molecule^{-1} s^{-1}, α is the saturation value (unitless), ϕ is the UV-photon flux in photons cm^{-2} s^{-1}, σ is the effective formation cross section in cm^2 photon^{-1}, and t is the experimental time in seconds. The rate constant (k) cannot be derived here due to the IR-inactive H_2, but the formation cross section (σ) is available from experimental results (Gerakines et al. 1996; Öberg et al. 2009; Oba et al. 2018). The derived fitting parameters are plotted in Figs. 4 and 5. In Fig. 4, the relative intensity of the saturation value (α), that is the final yield of HCO (black column) and DCO (red column), is presented for experiments of CO:H_2 and CO:D_2, respectively, after 60 min of UV-photon irradiation for temperatures in the range from 8 to 20 K. The unwanted contributions of HCO (white column) from residual H_2 and H_2O gas in the UHV chamber (as shown in Fig. 1) can be independently quantified in the CO:D_2 experiments and subtracted from the final HCO production in the CO:H_2 experiments. The derived relative HCO abundance with respect to the maximum yield, namely, the total HCO abundance before subtracting the unwanted HCO contributions, obtained at 8 K is ~0.74, ~0.48, ~0.40, ~0.29, and ~0.05 at 8, 10, 12, 14, and 20 K, respectively. The DCO abundance with respect to the HCO abundance at 8 K is ~0.12 and ~0.07 at 8 and 10 K, respectively. At 12 K, the DCO formation ratio, ~0.01, is only regarded as an upper limit due to low signal-to-noise ratio from the corresponding RAIRS signal.

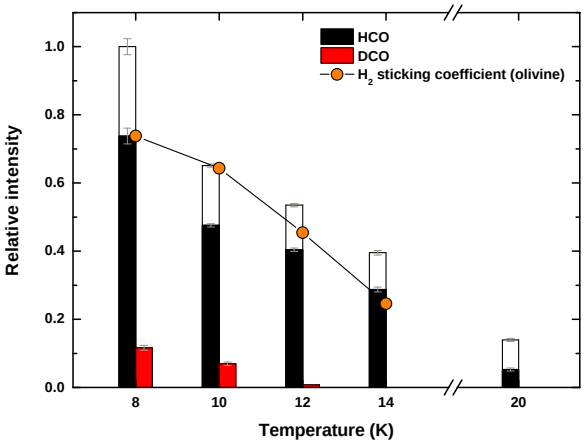

Fig. 4. Relative intensity of the final yield for N(HCO) (black column) and N(DCO) (red column), i.e., the saturation value (α), obtained after CO:H_2 and CO:D_2 ice UV irradiation for 60 min with a flux of 6×10^{12} photons cm^{-2} s^{-1} at temperatures ranging from 8 to 20 K, respectively. The white columns are the initial N(HCO) before subtraction of the extra HCO contribution from the contamination of residual H_2 or H_2O in the UHV chamber. The column densities have been calibrated by the initial CO ice thickness, and further normalized to the maximum ΔN(HCO) in the CO:H_2 experiment at 8 K, i.e., 2.5×10^{14} molecules cm^{-2}. The orange points are the reported relative intensity of H_2 sticking coefficients on olivine substrate at 8–14 K in Acharyya (2014).

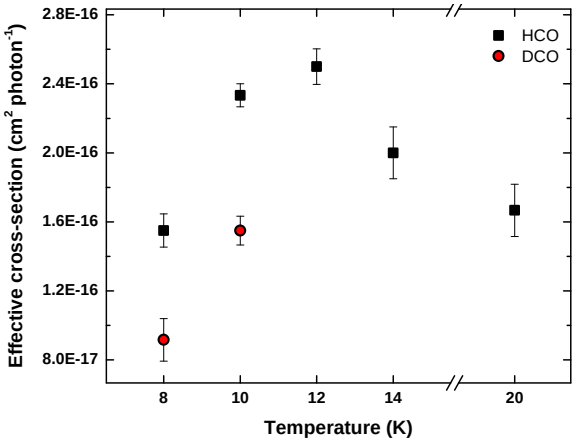

Fig. 5. Derived effective formation cross section (σ) obtained by fitting the kinetics of N(HCO) and N(DCO) formation over 60 min irradiation of UV-photons with a flux of 6×10^{12} photons cm^{-2} s^{-1} in experiments CO:H_2 and CO:D_2 at temperatures in the range from 8 to 20 K, respectively.

In Fig. 4, the calibrated HCO abundances show a strong temperature dependence at 8–20 K that can be linked to the relative sticking coefficient of H_2 reported in literature, for example, Acharyya (2014) on olivine substrate. This is also shown in the figure. Clearly our results and the data points reported by Acharyya (2014) are very similar. It should be noted, though, that the surface in our work, CO ice, is different from the substrate used in Acharyya (2014). As aforementioned, due to the lack of H_2 sticking coefficients on pure CO ice, the value reported for a non-water surface is currently the best option to compare with our experimental results. It reflects that the HCO formation abundance is predominantly controlled by the initial H_2 abundance in the pre-deposited CO:H_2 ice mixture. The H_2 abundance decreases with increasing temperature due to the dramatic drop of the sticking coefficient while the CO abundance (sticking coefficient = unity) remains constant at all experimental temperatures below 20 K. Up to our knowledge, the D_2 sticking coefficient on any surfaces at temperatures in the range of 8–20 K is not available from the literature. However, a similar correlation between the initial D_2 ice abundance and the final DCO yield is expected.

The formyl radical formation as result of UV-irradiation clearly shows an isotope effect in the overall formation yield; the HCO formation yield for UV irradiated CO:H_2 ice is about 6–7 times higher than the corresponding amount of DCO in CO:D_2 ices. This observation is not directly in line with the assumption of a higher sticking coefficient for D_2 compared to H_2, namely, the initial amount of frozen D_2 for a specific temperature is expected to be higher than for H_2 due to the higher binding energies for D_2 (Amiaud et al. 2015). The observed difference in the formation yield between the CO:H_2 and CO:D_2 will be discussed in the next section.

Figure 5 presents the effective formation cross section (σ), which is derived by the single exponential fit (i.e., Eq. (1)) of HCO and DCO formation kinetics for product HCO (black squares) and DCO (red dots). The derived cross section is the cumulative outcome of multiple reaction channels of HCO (DCO), and is believed to be mainly controlled by two reaction parameters, such as diffusion rate and sticking coefficient (initial ice abundance). Figure 5 shows a temperature-dependency of the HCO formation rate in the range of 8–20 K, with a maximum value at ~12 K. A proportional correlation, namely, increasing the ice sample temperature results in an increased formation cross section, in the range of 8–12 K; at 12 K the effective cross section of HCO is 1.7 times higher than the value at 8 K. One of the possible interpretations is that this positive slope can be explained by the diffusion rate that is expected to be also temperature dependent, namely, the higher the temperature, the higher the diffusion rate of H(D)-atoms is (Fuchs et al. 2009). However, at the same time, the formation cross section is also dominated by the available H_2 (D_2) ice abundance (species concentration in bulk ice) that is controlled by its sticking coefficient. At higher temperature, the concentration of H_2 (D_2) molecules in the CO ice is lower than that at low temperature. This results in a decreased effective cross section with increasing temperature from 2.5×10^{-16} at 12 K to 1.7×10^{-16} cm^2 photon^{-1} at 20 K (i.e., 68% less). A detailed temperature-dependent study (e.g., a wider temperature range and a better temperature resolution) is needed for a more detailed picture. For DCO, as aforementioned, the absolute formation yield above 12 K cannot be derived from the IR spectrum due to the limited detection sensitivity. With much thicker ice than used in this work, the effective formation cross section for higher temperature can be measured and also for CO:D_2 ices but this is presently outside the scope of this work. A similar temperature dependence of the formation rate due to the different sticking coefficients was reported in previous laboratory studies of CO hydrogenation in the same temperature range of 8–20 K (Watanabe et al. 2006).

3.3. H_2CO formation

Figure 6a shows the IR difference spectra obtained after UV irradiation of pre-deposited CO:H_2 for 240 min with a flux of 6×10^{12} photons cm^{-2} s^{-1} at 8 K. As aforementioned, HCO is observed at 1859 cm^{-1} along with 2488 and 1090 cm^{-1}, and its abundance is relatively stable in the range from 60 to 240 min. The new IR feature appearing at 1737 cm^{-1} can be assigned to monomer H_2CO (ν_2), and becomes much clearer with longer UV-photon irradiation time (Khoshkhoo & Nixon 1973; Nelander 1980). In Fig. 6b, the product abundances

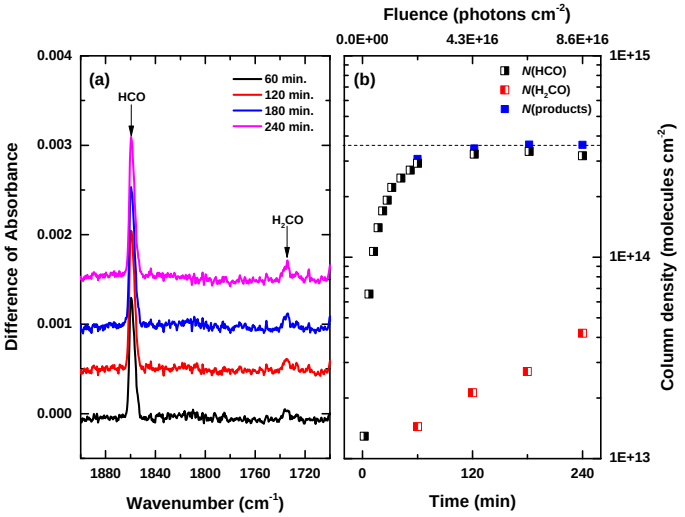

Fig. 6. *Left panel*: IR difference spectra of the UV photolysis of pre-deposited CO:H_2 ice with a photon-flux of 6×10^{12} photons cm^{-2} s^{-1} for 240 min at 8 K. *Right panel*: evolution of newly formed N(HCO) and N(H_2CO) and total abundance of photo-induced products over 240 min of UV-photon irradiation.

obtained from the integration of HCO (1859 cm^{-1}) and H_2CO (1737 cm^{-1}) IR signals, respectively, are presented over 240 min. The HCO formation rate starts slowing down after 60 min and slightly decreases after passing the maximum column density of 3×10^{14} molecules cm^{-2}. The detectable abundance of H_2CO builds up after 60 min of UV-irradiation as the fluence amounts to 2.2×10^{16} photons cm^{-2}, and the final abundance ratio of $\Delta N(H_2CO)/\Delta N(HCO)$ is ~0.13 reflecting that H_2CO is a second-generation product after HCO. The sum of N(HCO) and N(H_2CO) shows a relatively constant value of 3.6×10^{14} after 120 min suggesting a direct chemical link between these two products.

4. Discussion

The UV-photon energy applied here is ≤10.2 eV, and cannot directly dissociate CO or H_2 molecules; the required threshold dissociation energies of CO and H_2 in the gas phase are 11.09 and 11.20 eV, respectively (Field et al. 1966; Dalgarno & Stephens 1970; Okabe 1978). In the solid state these values can decrease, but with 0.13 eV decrease for CO the effect is negligible (Lu et al. 2005). However, CO has a strong absorption cross section in the 127–157 nm range, coinciding with the wavelength of the impacting UV-photons. This allows to excite CO into its first electronic state ($A^1\Pi \longleftarrow X^1\Sigma^+$), namely, CO* with excess energy ≥ 7.9 eV (Lu et al. 2005; Mason et al. 2006; Cruz-Diaz et al. 2014);

$$CO + h\nu \longrightarrow CO^*. \quad (2)$$

Subsurface CO* can transfer the energy to the top layer molecules leading to the CO non-thermal desorption at low temperature, as discussed by Fayolle et al. (2011) and van Hemert et al. (2015), and in the bulk it can further react with neighboring CO to form CO_2 (Okabe 1978; Gerakines et al. 1996; Gerakines & Moore 2001; Loeffler et al. 2005; Bertin et al. 2013; Chen et al. 2014);

$$CO^* + CO \longrightarrow CO_2 + C. \quad (3)$$

Due to a small amount of H_2O contamination as shown in our IR spectrum at 1600 cm^{-1}, another reported CO_2 formation channel through the reaction between CO and OH radical, originating from H_2O photodissociation, cannot be excluded (Watanabe & Kouchi 2002; Watanabe et al. 2007; Oba et al. 2010; Ioppolo et al. 2011).

As mentioned, the H_2 (D_2) molecule cannot be directly dissociated in H-atoms (D-atoms) upon Lyα irradiation, or electronically excited by a UV-photon (≤ 10.2 eV), however, an alternative channel may apply that is similar to the CO_2 formation scheme shown in Eq. (3):

$$CO^* + H_2 \longrightarrow HCO + H_{dis}. \quad (4)$$

The lowest potential energy of the first electronic state of CO is 7.9 eV, and is larger than the reported enthalpy of CO+H_2 ⟶HCO+H in the gas phase, that is ~3.7 eV (Reilly et al. 1978). Moreover, ab initio calculations show that the H_2 dissociation due to energy transfer from the electronically excited CO is a barrierless reaction (Sperlein et al. 1987). Therefore, we expect that the reaction shown in Eq. (4) proceeds without activation barrier in the solid state as well. The product HCO is likely thermally stabilized below 20 K, and preserved in the ice mixture. The free H-atom (H_{dis}) that is formed in Eq. (4) may react with the newly formed HCO radical in Eq. (4) yielding H_2CO or CO+H_2 through

$$H_{dis} + HCO \longrightarrow H_2CO \quad (5a)$$

$$H_{dis} + HCO \longrightarrow CO + H_2. \quad (5b)$$

There is also a possibility that the H_{dis} diffuses in the bulk ice and reacts with CO to form HCO through direct H-atom addition reactions contributing to the total yield of HCO detected in the IR spectrum (Watanabe & Kouchi 2002; Fuchs et al. 2009):

$$H_{dis} + CO \longrightarrow HCO, \quad (6)$$

or meets with other free radicals available in the ice, like HCO and H_{dis} forming H_2CO (Eq. 5a), H_2+CO (EQ. 5b) and H_2 through

$$H_{dis} + H_{dis} \longrightarrow H_2. \quad (7)$$

The reaction channels of Eqs. (5)–(7) compete with each other showing a strong temperature dependence due to the different diffusion rates; at higher ice temperatures, the mobile H-atom will diffuse away much quicker from the newly formed HCO in the bulk ice, and eventually react with CO forming HCO. This may explain the increase of the observed HCO formation cross section in Fig. 5 at temperatures from 8 to 12 K. Beyond 12 K, the substantial decrease of the effective concentration of H_2 leads to a lower cumulative formation rate.

For the final yield of HCO, it is important to note that the HCO formation in Eq. (4) induced by UV-photons is expected to proceed without activation barrier, but the hydrogenation of CO in Eq. (6) was shown before to exhibit a strong isotope effect due to the quantum tunneling of H(D)-atoms (Hidaka et al. 2007). This likely explains the difference in formation yield between HCO and DCO, and shows that secondary D(H)-atoms are indeed contributing to the overall abundances. Therefore, the derived formation cross section of formyl radical is concluded to be an effective value that is controlled by the reaction parameters, such as sticking coefficient, diffusion rate for H_2 and D_2 molecules, and an isotope effect that gets important in a secondary reaction step.

The possible formation mechanism of H_2CO is through the reaction HCO+H, of which the H-atom can be directly formed as shown in Eq. (4) or be produced by photodissociation of HCO (Heays et al. 2017):

$$HCO + h\nu \longrightarrow CO + H. \quad (8)$$

Alternatively, the interaction between two HCO radicals can result in their recombination into glyoxal or H_2CO and CO formation through the reaction (Butscher et al. 2017):

$$HCO + HCO \longrightarrow H_2CO + CO. \quad (9)$$

In this work, the observed H_2CO formation is found when HCO abundance passes its maximum yield and starts decreasing (Fig. 6), implying that the HCO is a key precursor to form H_2CO in present study.

We note that the interaction of UV-photons and a metallic substrate (gold; work function = 4.4 eV) may result in photoelectrons. These are expected to have a limited penetration depth in condensed ices, namely, few layers at maximum (Jo & White 1991). To proof this assumption, a control experiment with a thick layer of Ar ice (~20 Langmuir) between gold substrate and CO:H_2 ice mixture has been performed. After applying the same fluence of UV-photon irradiation, the same absolute production yield of HCO is found; this implies that indeed any additional contribution from photo-induced electrons interacting with the CO:H_2 ice mixture will be negligible.

5. Astrochemical implication

This laboratory work shows that electronically excited ice species induced by UV-photons can react with H_2 molecules adsorbed (or trapped) in interstellar ices at low temperatures to form new species. In space, cosmic rays, electrons, and photons can all interact with the ice mantle resulting in energy transfer. Such events can lead to a series of different thermal and chemical processes depending on the energetic input and chemical composition of the ice. For instance, previous laboratory studies on UV-irradiation of CO ice showed that although UV-photons cannot photodissociate CO molecules, they can electronically excite CO^* species that can then cause the non-thermal desorption of other CO molecules (Fayolle et al. 2011; van Hemert et al. 2015). This mechanism successfully explains the observed gaseous abundance of CO at low temperature and also, at least partially, the photo-excitation chemistry resulting in the formation of C_nO_m species in the solid phase, particularly CO_2 (Gerakines & Moore 2001; Loeffler et al. 2005). It also has been linked to the location of photo-induced snow lines in proto-planetary disks (Qi et al. 2015; Öberg et al. 2015).

In dense clouds, the H_2 abundance is four orders of magnitude higher than that of H-atoms. Therefore, since H_2 molecules are expected to be found in interstellar ices at low temperatures (Sandford et al. 1993; Buch & Devlin 1994; Dissly et al. 1994), it is possible that electronically excited species react with molecular hydrogen getting hydrogenated. The decomposition of H_2 induced by the excited species results in a free H-atom that can further hydrogenate other molecules forming hydrogen-saturated species, like CH_3OH and COMs. This mechanism may also apply to other reaction chains. For instance, water and hydrocarbons can be formed through reactions of hydrogen molecules with photo-excited oxygen-atoms (O^*) and carbon-atoms (C^*), respectively. Both have a strong UV-photon absorption cross section in the range of 120–160 nm.

It should be noted that the solid-state formation of hydrogen-rich species containing atomic C and O (e.g., H_2CO and CH_3OH) is believed to occur predominantly through H-atom addition reactions to CO in dense clouds. In the present work we show for a first time that electronically excited species can react with frozen H_2 under dense cloud conditions, a process that is limitedly involved in current astrochemical networks. We propose a general mechanism on the example of CO:H_2+hν as this system is well studied and has a minimum number of competing side-photochemical products. It offers an additional channel that holds the potential to form HCO radicals (and larger species) in interstellar ices, especially at very low temperatures. Since there is no proof of CH_3OH formation in our experiments, this hints at a lower efficiency of the CO^*+H_2 compared to the regular CO+H hydrogenation chain. As UV light can penetrate deeper in ices than H-atoms, the mechanism studied here may increase the abundance of HCO radicals in the deeper layers of the ice, where CO and H_2 (depending on temperature) are preserved and H-atoms cannot penetrate. Ultimately, this may affect the efficiency with which COMs can be formed in the later stage when the ice mantle is gently heated by the central protostar. The work presented here should be considered as a case study, investigating a new process capable of triggering chemical reactions at low temperatures in interstellar ices. The process may be more generally relevant, and applicable to other reaction chains as well. To which extent such reaction routes contribute to the full chemical picture, will be topic of future astrochemical modeling studies.

6. Conclusions

Below are given the main findings of this experimental study for frozen H_2 when adsorbed or trapped in interstellar ice analogues upon UV irradiation:

1. UV-photons generated by cosmic rays in dense clouds may increase HCO (H_2CO and possibly larger COMs) abundances by triggering a solid-state reaction involving electronically excited CO^* and H_2. The HCO formation is explained by two consecutive reaction steps CO^*+$H_2 \longrightarrow$ HCO+H_{dis} and CO+$H_{dis} \longrightarrow$ HCO.
2. The derived effective formation cross section shows a temperature dependence that is determined by the cumulative effect of the H-atom diffusion rate and initial H_2 concentration in the bulk ice that is determined by the sticking coefficient. For the investigated laboratory settings, we find a maximum at 12 K of 2.5×10^{-16} cm^2 photon^{-1}.
3. The surface temperature between 8 and 20 K determines the photolysis product yield and this is due to the temperature-dependent sticking efficiency of H_2.
4. The mechanism that involves reactions between electronically excited species and H_2 molecules on icy grains may be of more general importance in ISM chemistry. It will take more detailed astrochemical modeling to put this pathway into perspective and to check to which extent this contributes to the formation of H_2CO and eventual COMs in space. Based on the experiments performed here, the mechanism is found to contribute, but very likely at a level that is (substantially) lower than regular CO hydrogenation upon impacting H-atoms.

Acknowledgements. This research was funded through a VICI grant of NWO (the Netherlands Organization for Scientific Research), an A-ERC grant 291141 CHEMPLAN, and has been performed within the framework of the Dutch Astrochemistry Network. Financial support by NOVA (the Netherlands Research School for Astronomy) and the Royal Netherlands Academy of Arts and Sciences (KNAW) through a professor prize is acknowledged. G.F. acknowledges the financial support from the European Union's Horizon 2020 research and innovation program under the Marie Sklodowska-Curie grant agreement no. 664931. S.I. acknowledges the Royal Society for financial support and the Holland Research School for Molecular Chemistry (HRSMC) for a travel grant. The described work has benefited a lot from continuing collaborations within the framework of the FP7 ITN LASSIE consortium (GA238258) We thank M. van Hemert and T. Lamberts for stimulating discussions.

References

Acharyya, K. 2014, MNRAS, 443, 1301
Amiaud, L., Fillion, J.-H., Dulieu, F., Momeni, A., & Lemaire, J.-L. 2015, Phys. Chem. Chem. Phys., 17, 30148
Bacmann, A., Taquet, V., Faure, A., Kahane, C., & Ceccarelli, C. 2012, A&A, 541, L12
Balucani, N., Ceccarelli, C., & Taquet, V. 2015, MNRAS, 449, L16
Bennett, C. J., Chen, S.-H., Sun, B.-J., Chang, A. H. H., & Kaiser, R. I. 2007, ApJ, 660, 1588
Bertin, M., Fayolle, E. C., Romanzin, C., et al. 2013, ApJ, 779, 120
Bertin, M., Romanzin, C., Doronin, M., et al. 2016, ApJ, 817, L12
Boogert, A. C. A., Gerakines, P. A., & Whittet, D. C. B. 2015, ARA&A, 53, 541
Borget, F., Müller, S., Grote, D., et al. 2017, A&A, 598, A22
Buch, V., & Devlin, J. P. 1994, ApJ, 431, L135
Butscher, T., Duvernay, F., Theule, P., et al. 2015, MNRAS, 453, 1587
Butscher, T., Duvernay, F., Danger, G., & Chiavassa, T. 2016, A&A, 593, A60
Butscher, T., Duvernay, F., Rimola, A., Segado-Centellas, M., & Chiavassa, T. 2017, Phys. Chem. Chem. Phys., 19, 2857
Cernicharo, J., Marcelino, N., Roueff, E., et al. 2012, ApJ, 759, L43
Chang, Q. & Herbst, E. 2012, ApJ, 759, 147
Charnley, S. B. 1997, MNRAS, 291, 455
Chen, Y.-J., Chuang, K.-J., Muñoz Caro, G. M., et al. 2014, ApJ, 781, 15
Chervenak, J. & Anderson, R. 1971, JOSA, 61, 952
Chuang, K.-J., Fedoseev, G., Ioppolo, S., van Dishoeck, E. F., & Linnartz, H. 2016, MNRAS, 455, 1702
Chuang, K.-J., Fedoseev, G., Qasim, D., et al. 2017, MNRAS, 467, 2552
Chuang, K.-J., Fedoseev, G., Qasim, D., et al. 2018, ApJ, 853, 102
Cruz-Diaz, G. A., Muñoz Caro, G. M., Chen, Y.-J., & Yih, T.-S. 2014, A&A, 562, A119
Cuppen, H. M., van Dishoeck, E. F., Herbst, E., & Tielens, A. G. G. M. 2009, A&A, 508, 275
Cuppen, H. M., Ioppolo, S., Romanzin, C., & Linnartz, H. 2010, Phys. Chem. Chem. Phys., 12, 12077
Dalgarno, A. & Stephens, T. L. 1970, ApJ, 160, L107
Dissly, R. W., Allen, M., & Anicich, V. G. 1994, ApJ, 435, 685
Dulieu, F., Amiaud, L., Congiu, E., et al. 2010, A&A, 512, A30
Ewing, G. E., Thompson, W. E., & Pimentel, G. C. 1960, J. Chem. Phys., 32, 927
Fayolle, E. C., Bertin, M., Romanzin, C., et al. 2011, ApJ, 739, L36
Fedoseev, G., Cuppen, H. M., Ioppolo, S., Lamberts, T., & Linnartz, H. 2015, MNRAS, 448, 1288
Fedoseev, G., Chuang, K.-J., van Dishoeck, E. F., Ioppolo, S., & Linnartz, H. 2016, MNRAS, 460, 4297
Fedoseev, G., Chuang, K.-J., Ioppolo, S., et al. 2017, ApJ, 842, 52
Field, G. B., Somerville, W. B., & Dressler, K. 1966, ARA&A, 4, 207
Fuchs, G. W., Cuppen, H. M., Ioppolo, S., et al. 2009, A&A, 505, 629
Garrod, R. T. 2013, ApJ, 778, 158
Garrod, R., Park, I. H., Caselli, P., & Herbst, E. 2006, Faraday Discuss., 133, 51
Gerakines, P. A. & Moore, M. H. 2001, Icarus, 154, 372
Gerakines, P. A., Schutte, W. A., Greenberg, J. M., & van Dishoeck E. F. 1995, A&A, 296, 810
Gerakines, P. A., Schutte, W. A., & Ehrenfreund, P. 1996, A&A, 312, 289
Hama, T. & Watanabe, N. 2013, Chem. Rev., 113, 8783
Heays, A., Bosman, A. D., & van Dishoeck, E. 2017, A&A, 602, A105
Hidaka, H., Kouchi, A., & Watanabe, N. 2007, J. Chem. Phys., 126, 204707
Hidaka, H., Watanabe, M., Kouchi, A., & Watanabe, N. 2009, ApJ, 702, 291
Hiraoka, K., Miyagoshi, T., Takayama, T., Yamamoto, K., & Kihara, Y. 1998, ApJ, 498, 710
Ioppolo, S., Cuppen, H. M., Romanzin, C., van Dishoeck, E. F., & Linnartz, H. 2008, ApJ, 686, 1474
Ioppolo, S., Cuppen, H. M., Romanzin, C., van Dishoeck, E. F., & Linnartz, H. 2010, Phys. Chem. Chem. Phys., 12, 12065
Ioppolo, S., van Boheemen, Y., Cuppen, H. M., van Dishoeck, E. F., & Linnartz, H. 2011, MNRAS, 413, 2281
Ioppolo, S., Fedoseev, G., Lamberts, T., Romanzin, C., & Linnartz, H. 2013, Rev. of Sci. Instrume., 84, 073112
Jiménez-Serra, I., Vasyunin, A. I., Caselli, P., et al. 2016, ApJ, 830, L6
Jo, S. K. & White, J. 1991, J. Chem. Phys., 94, 5761
Khoshkhoo, H. & Nixon, E. R. 1973, Spectrochim. Acta A: Mol. Spectr., 29, 603
Kristensen, L., Amiaud, L., Fillion, J.-H., Dulieu, F., & Lemaire, J.-L. 2011, A&A, 527, A44
Lamberts, T., Cuppen, H. M., Ioppolo, S., & Linnartz, H. 2013, Phys. Chem. Chem. Phys., 15, 8287
Lamberts, T., Cuppen, H. M., Fedoseev, G., et al. 2014, J. Vac. Sci. Technol., 570, A57
Lee, T. J. 1972, J. Vac. Sci. Technol., 9, 257
Ligterink, N. F. W., Paardekooper, D. M., Chuang, K.-J., et al. 2015, A&A, 584, A56
Ligterink, N., Walsh, C., Bhuin, R., et al. 2018, A&A, 612, A88
Linnartz, H., Ioppolo, S., & Fedoseev, G. 2015, Int. Rev. Phys. Chem., 34, 205
Loeffler, M. J., Baratta, G. A., Palumbo, M. E., Strazzulla, G., & Baragiola, R. A. 2005, A&A, 435, 587
Lu, H.-C., Chen, H.-K., Cheng, B.-M., Kuo, Y.-P., & Ogilvie, J. F. 2005, J. Phys. B At. Mol. Phys., 38, 3693
Mason, N. J., Dawes, A., Holtom, P. D., et al. 2006, Faraday Discuss., 133, 311
Matar, E., Bergeron, H., Dulieu, F., et al. 2010, J. Chem. Phys., 133, 104507
Meisner, J., Lamberts, T., & Kästner, J. 2017, ACS Earth Space Chem., 1, 399
Mennella, V., Baratta, G. A., Esposito, A., Ferini, G., & Pendleton, Y. J. 2003, ApJ, 587, 727
Milligan, D. E. & Jacox, M. E. 1964, J. Chem. Phys., 41, 3032
Miyauchi, N., Hidaka, H., Chigai, T., et al. 2008, Chem. Phys. Lett., 456, 27
Muñoz Caro, G. M., Jiménez-Escobar, A., Martín-Gago, J. Á., et al. 2010, A&A, 522, A108
Nelander, B. 1980, J. Chem. Phys., 73, 1026
Oba, Y., Miyauchi, N., Hidaka, H., et al. 2009, ApJ, 701, 464
Oba, Y., Watanabe, N., Kouchi, A., Hama, T., & Pirronello, V. 2010, ApJ, 712, L174
Oba, Y., Watanabe, N., Hama, T., et al. 2012, ApJ, 749, 67
Oba, Y., Tomaru, T., Lamberts, T., Kouchi, A., & Watanabe, N. 2018, Nat. Astron., 2, 228
Öberg, K. I., Garrod, R. T., van Dishoeck, E. F., & Linnartz, H. 2009, A&A, 504, 891
Öberg, K. I., Bottinelli, S., Jørgensen, J. K., & van Dishoeck E. F. 2010, ApJ, 716, 825
Öberg, K. I., Furuya, K., Loomis, R., et al. 2015, Astrophys. J., 810, 112
Okabe, H. 1978, Photochemistry of small molecules (New York: Wiley)
Paardekooper, D. M., Fedoseev, G., Riedo, A., & Linnartz, H. 2016, A&A, 596, A72
Pontoppidan, K. M. 2006, A&A, 453, L47
Prasad, S. S. & Tarafdar, S. P. 1983, ApJ, 267, 603
Qi, C., Öberg, K. I., Andrews, S. M., et al. 2015, ApJ, 813, 128
Reilly, J., Clark, J., Moore, C. B., & Pimentel, G. C. 1978, J. Chem. Phys., 69, 4381
Sandford, S. A. & Allamandola, L. J. 1993, ApJ, 409, L65
Sandford, S. A., Allamandola, L. J., & Geballe, T. R. 1993, Science, 262, 400
Shen, C. J., Greenberg, J. M., Schutte, W. A., & van Dishoeck E. F. 2004, A&A, 415, 203
Sperlein, R. F., Golde, M. F., & Jordan, K. D. 1987, Chem. Phys. Lett., 142, 359
Tielens, A. G. G. M. & Hagen, W. 1982, A&A, 114, 245
Tobias, I., Fallon, R. J., & Vanderslice, J. T. 1960, J. Chem. Phys., 33, 1638
van Hemert, M. C., Takahashi, J., & van Dishoeck, E. F. 2015, J. Phys. Chem. A, 119, 6354
Vidali, G. 2013, Chem. Rev., 113, 8762
Wakelam, V., Bron, E., Cazaux, S., et al. 2017, Mol. Astrophys., 9, 1
Warren, J. A., Smith, G. R., & Guillory, W. A. 1980, J. Chem. Phys., 72, 4901
Watanabe, N. & Kouchi, A. 2002, ApJ, 571, L173
Watanabe, N. & Kouchi, A. 2008, Prog. Surf. Sci., 83, 439
Watanabe, N., Nagaoka, A., Hidaka, H., et al. 2006, Planet. Space Sci., 54, 1107
Watanabe, N., Mouri, O., Nagaoka, A., et al. 2007, ApJ, 668, 1001
Wooden, D. H., Charnley, S. B., & Ehrenfreund, P. 2004, Composition and Evolution of Interstellar Clouds, ed. G. W. Kronk, 33
Woods, P. M., Kelly, G., Viti, S., et al. 2012, ApJ, 750, 19